

Interface Engineering in Heteroepitaxy

S.K. HONG, Y. CHEN, H.J. KO AND T. YAO

Institute for Materials Research, Tohoku University, Sendai 980-8577, Japan

We report the importance of interface engineering in heteroepitaxy with examples of plasma-assisted molecular beam epitaxial ZnO growths on (0001) sapphire substrates and on (0001) GaN/sapphire templates, whose interfaces are engineered to improve and to control properties of ZnO films. The growth of rocksalt structure MgO buffer on Al₂O₃ (0001) is developed for ZnO epitaxy. By employing the MgO buffer layer, the formation of 30° rotated mixed domains is prohibited and two-dimensional layer-by-layer growth of ZnO on sapphire substrate is achieved. High-resolution X-ray diffraction reveals the superior improvement in a crystal quality of ZnO films with an MgO buffer. Polarity of wurtzite structure ZnO films on Ga-polar GaN/sapphire templates is controlled by changing interface structures. By forming a single crystalline, monoclinic Ga₂O₃ interfacial layer between GaN and ZnO through O-plasma pre-exposure on the Ga-polar GaN surface, O-polar ZnO films are grown. By forming the ZnO/GaN heterointerface without an interfacial layer through the Zn pre-exposure on the Ga-polar GaN surface, Zn-polar ZnO films are grown.

PACS numbers: 68.35.-p, 68.35.Dv, 81.15.-z, 81.15.Hi, 81.10.Aj

1. Introduction

ZnO, one of wide band gap semiconductors, has been revealed that this material is promising for exciton-based photonic devices in the ultra-violet region [1–3]. The absence of a suitable substrate for ZnO epitaxy is an emerging issue in ZnO epitaxy. Homoepitaxy may provide a promising solution for this issue and commercial ZnO substrates are being supplied. Several benefits of homoepitaxy, such as (1) perfect lattice matching, (2) no thermal mismatch, (3) no crystallographic mismatch, and (4) simple control of lattice polarity by using different-polar substrates, are expected. However, crystal qualities of the ZnO substrate are far from those applicable to ZnO epitaxy for devices [4].

Al₂O₃ (0001), one of the most popular oxide substrates, has widely been used for the substrate for ZnO epitaxy. However, there are considerable mismatches in this heteroepitaxy system including large lattice misfit of 18.6%, crystallographic

mismatch, and thermal mismatch. Those mismatches have caused various problems including a highly disordered heterointerface, a formation of 30°-rotated domains, and degraded crystallinity of ZnO layers [5]. Recent achievements in heteroepitaxy of wide band gap semiconductors on highly mismatched substrates largely rely on how well a template is created in between the epilayer and the substrate [6]. Therefore, the exploring and development of epitaxy technique, which can provide a suitable template for ZnO epitaxy, are highly needed for ZnO epitaxy on *c*-plane sapphire considering the mismatches in the system.

As a non-oxide substrate, GaN is an attractive material applicable as a substrate for ZnO epitaxy. In the case of a ZnO/GaN system, there are several merits compared with the ZnO/sapphire: (1) smaller lattice misfit (1.9%), (2) no crystallographic mismatch, and (3) smaller thermal mismatch. Although there are such merits in using GaN as a substrate for the ZnO epitaxy, the getting of the high quality GaN substrates is as difficult as the case for ZnO. Fortunately, the recent progress in metal organic chemical vapor deposition (MOCVD) of GaN on *c*-plane sapphire can provide a relatively high quality of GaN template substrate on sapphire, which can be used as a substrate for ZnO epitaxy. Because the polarity of such high-quality MOCVD GaN is typical of Ga-polar and both ZnO and GaN are of wurtzite structure, the polarity of ZnO films on GaN may reflect the polarity of underlying GaN. Therefore, a selective growth of Zn- and O-polar ZnO films on Ga-polar GaN is an attractive issue for the progress of heteroepitaxy in material systems of wurtzite structure.

In this article, the importance of interface engineering in heteroepitaxy is demonstrated, the concept of which can be applied to other material systems, with our recent results of (1) drastic improvement in crystal qualities of ZnO films on *c*-plane sapphire by using a novel MgO buffer layer [7, 8] and (2) control of ZnO film polarities on Ga-polar GaN templates by controlling interface formations [9, 10].

2. Experimental

2.1. ZnO on Al₂O₃ (0001)

Commercial Al₂O₃ (0001) substrates were used. Reflection high-energy electron diffraction (RHEED) was used to monitor the growth procedures. The deposition of MgO buffer layer is carried out at 480°C with a slow deposition rate of about 0.01 Å/s under oxygen rich conditions. We found that a low growth rate is critical to the formation of an MgO wetting layer on the Al₂O₃ (0001) surface. After the deposition of a nominal 2 nm thick MgO buffer, ZnO growth is carried out at 480°C for a few minutes and an annealing at 750°C under the exposure of oxygen plasma for 5 minutes is performed. The subsequent growth of the ZnO is then carried out at a temperature of 650°C, with a Zn beam flux around 0.22 nm/s and oxygen flow rate of 1.5 sccm under the plasma power of 300 W. RHEED inten-

sity oscillations using the specular spot can be recorded during this growth stage. X-ray diffraction (XRD) was used to investigate the structural properties of the ZnO epilayers. To directly measure the buffer, thin ZnO layers were grown and grazing incident XRD was used for characterization.

2.2. ZnO on GaN template

4 μm -thick Ga-polar GaN epilayers grown by MOCVD on Al_2O_3 (0001) were used as templates for ZnO epitaxy. The GaN template was thermally cleaned at 700–750°C in ultra-high vacuum for about 1 h after being degreased in acetone and methanol. The Zn flux was set to about 0.15–0.20 nm/s and O-plasma conditions were set to 300–400 W of power with an oxygen gas flow rate of 3.5 sccm. The growth under these conditions gave a flux ratio that was oxygen rich. Two types of pre-growth treatments of the GaN surface were examined: (1) Zn pre-exposure for 2–3 min, and (2) O-plasma pre-exposure for 3–5 min. The interface structure was observed by high-resolution transmission electron microscopy (HRTEM) with a zone axis of $[2\bar{1}\bar{1}0]$. Identification of interfacial layer was performed using a digital diffraction pattern (DDP) obtained by fast Fourier transform (FFT) of the HRTEM image. The polarity of the ZnO films was determined by convergent beam electron diffraction (CBED). The CBED patterns were obtained at 100 keV with a 20-nm probe from several regions per sample with a zone axis of $[2\bar{1}\bar{1}0]$. Experimental CBED patterns from the ZnO and GaN layers were compared with simulated patterns for TEM specimen thicknesses of 10–80 nm to determine the polarity.

3. Results and discussion

3.1. ZnO films with MgO buffer on *c*-plane sapphire

Figure 1 shows the RHEED patterns recorded during the initial growth stages. At the very beginning of MgO deposition, a diffuse streaky pattern (Fig. 1a) evolves indicating the formation of an MgO wetting layer on the Al_2O_3 (0001) surface. According to the growth rate the evaluated thickness is between one and two monolayers. The continuing growth of MgO leads to diffused spotty patterns indicative of a transition to the island growth mode (Fig. 1b), which is caused by the near 9% in-plane lattice mismatch if MgO grows with its [111] axis normal to the Al_2O_3 (0001) plane. As the ZnO deposition starts, spotty patterns (Fig. 1c) with a rod spacing of about 9% smaller emerge superimposing on the MgO patterns. As the growth is continuing, ZnO patterns gradually take the places of the MgO pattern, and of the same time, the RHEED spots elongate and connect with each other. Finally, streaky RHEED patterns evolve. Such a procedure takes about one hour, corresponding to the deposition of a 200–300 nm thick film. In another approach, annealing at 700°C for about 5 min is carried out on the low tem-

perature grown ZnO layer with a thickness of around several nanometers. Sharp streaky RHEED patterns (Fig. 1d) were present after annealing. Comparing with the growth of ZnO on Al_2O_3 (0001) without the use of an MgO buffer, where a columnar growth usually takes place, the use of a MgO buffer successfully promotes the lateral growth of ZnO at an initial stage and a flat ZnO template is created for subsequent two-dimensional (2D) ZnO growth.

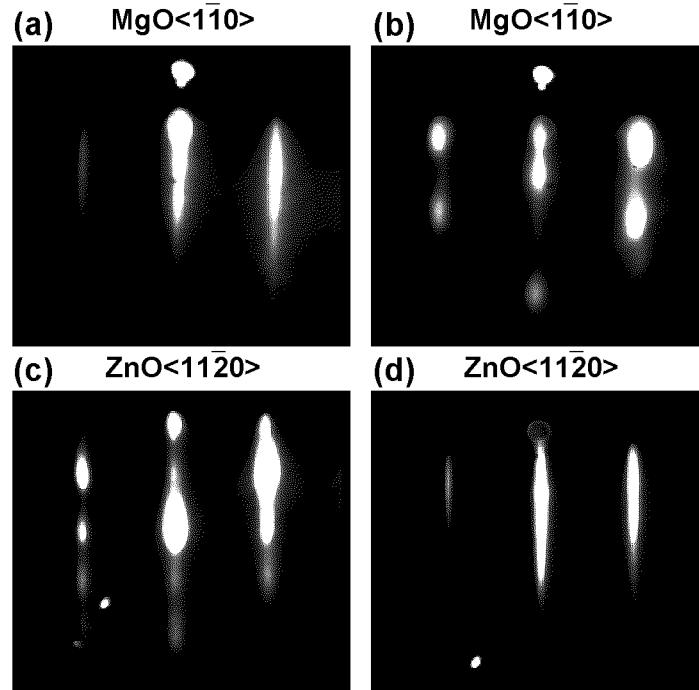


Fig. 1. RHEED patterns at different growth stages: (a) the MgO wetting layer on Al_2O_3 (0001) substrate, (b) the MgO buffer layer after a 2D–3D transition, (c) the ZnO layer grown at 480°C on the MgO buffer, (d) the ZnO layer after annealing at 750°C for 5 min.

As an evidence of 2D layer-by-layer growth, RHEED intensity oscillations are recorded during the consequent ZnO growth. Figure 2 shows the RHEED specular beam intensity oscillations with the incident electron beam along the ZnO $\langle 11\bar{2}0 \rangle$ azimuth at various growth temperatures. More than fifty oscillations are recorded at the growth temperature of 400°C , while only a few slight oscillations can be observed at 720°C . The fast damp of the RHEED oscillations at a higher growth temperature is due to the growth mode transition from 2D nucleation to step-flow mode but not to the surface morphology degrading, since the sharp streaky RHEED pattern with the intense specular spot becomes even clearer at higher temperatures.

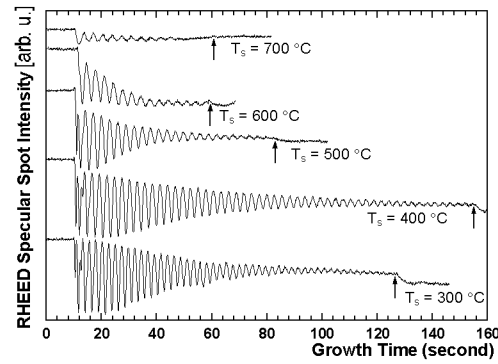


Fig. 2. RHEED specular spot intensity oscillations on the 00 rod in $\langle 11\bar{2}0 \rangle$ azimuth at various growth temperatures. Arrows indicate where the growth is interrupted.

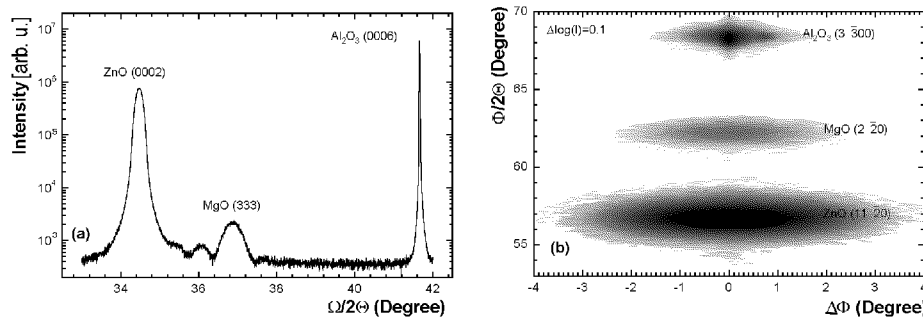


Fig. 3. (a) $\Omega-2\Theta$ scan along the surface normal of a thin ZnO epilayer grown on Al_2O_3 (0001) with an MgO buffer; (b) Grazing-incident XRD mapping of the in-plane diffraction peaks.

In order to identify the crystal structure of the buffer, an MgO layer about 7 nm, thicker than a usually used 2–3 nm buffer, was grown and covered by a 15 nm thick ZnO layer. The growth processes monitored by RHEED did not show any difference from a typical buffer, which allows us to use this sample for investigating the crystal structure of the MgO buffer. Figure 3a shows the XRD $\Omega-2\Theta$ scan along the surface normal of the sample. Besides the ZnO (0002) and the Al_2O_3 (0006) peaks, a diffraction peak at $2\Theta = 36.910^\circ$ is observed. After correcting the zero-error of the XRD diffractometer, an inter-plane distance of 0.2434 nm is obtained. This value corresponds to the distance between (333) planes in bulk MgO with a strain less than 0.07% indicating the fully relaxed MgO growth along [111] direction on Al_2O_3 (0001) substrate. The fringes confirm the thickness of the MgO layer of about 7 nm. The presence of interference fringes also indicates a sharp interface with little inter-diffusion. To get further information of the structural properties, grazing-incident XRD measurements were carried out. Figure 3b

shows the in-plane reciprocal space mapping. The rocksalt MgO ($2\bar{2}0$) peak appears in alignment with ZnO ($11\bar{2}0$) and Al₂O₃ ($3\bar{3}00$). Thus the in-plane epitaxial relationship is determined as ZnO[$1\bar{1}00$]/MgO[$1\bar{1}0$]/Al₂O₃[$11\bar{2}0$], consistent with the RHEED observation [7]. No other structural phases were observed by grazing-incident XRD measurements. Therefore, we can exclude the alloy formation from Al₂O₃/MgO/ZnO interfaces. We know that the oxygen sub-lattice with hexagonal (ZnO and Al₂O₃) or cubic (MgO) close-packed structure determines the lattice matching of two oxides. Therefore, the lattice mismatch is 18.6% and 8.3% for ZnO(0001)/Al₂O₃(0001) and MgO(111)/Al₂O₃(0001), respectively. The metal cations occupy either the tetragonal (Zn in ZnO) or the orthogonal (Al in Al₂O₃, and Mg in MgO) vacancy formed by oxygen anions, which leads to a chemical mismatch across the hetero-interface. The rocksalt MgO finds its in-plane lattice constant just at the intermediate position between that of ZnO and Al₂O₃, as well as its poly-covalent ionic bonding situation. This may explain why MgO wets Al₂O₃ and ZnO adhere to MgO. We should clarify that no improvement in morphology and crystal quality can be obtained if ZnO is grown directly on an MgO wetting layer. This is reasonable because the release of strain greatly contributes to lowering the surface energy and reducing the mismatch. Furthermore, the 2D-3D transition resulted islands provide nucleation cores for the following ZnO growth.

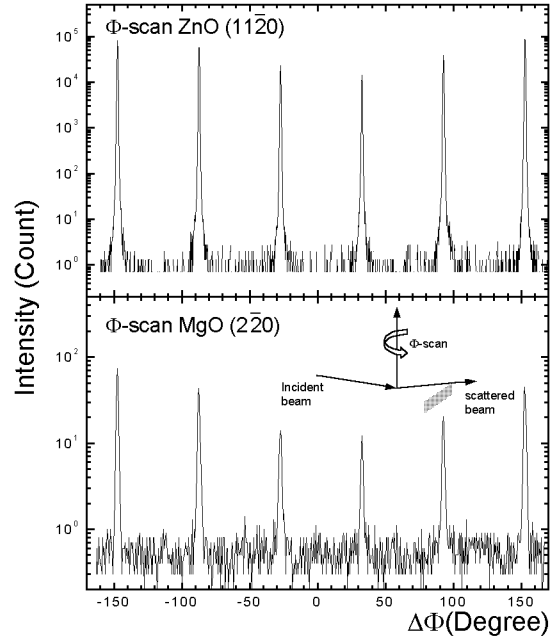


Fig. 4. Φ -scans of (a) ZnO ($11\bar{2}0$) and (b) MgO ($2\bar{2}0$) diffraction peaks show the in-plane epitaxial relationship. The insertion in (b) indicates the geometry of scan.

Figure 4 shows Φ -scan with an incident angle of 0.35° . MgO ($2\bar{2}0$) peaks are found coincident with ZnO ($11\bar{2}0$), which confirms again that MgO has a rock-salt structure and has the in-plane epitaxial relationship as ZnO[$1\bar{1}00$]/MgO[$1\bar{1}0$]/Al₂O₃[$11\bar{2}0$]. From these results, we speculate that the effect of MgO buffer is mainly in lowering the substrate surface energy, which is favorable to the lateral growth of ZnO. It should be strongly noted that Fig. 4 indicates six-fold rotational symmetry along the $\langle 0001 \rangle$ direction, which means there are no formation of 30° rotated mixed domains.

In Fig. 5 we compare the high-resolution XRD results taken from the ZnO epilayers grown on Al₂O₃ with and without an MgO buffer. Figure 5a shows the $\Omega-2\theta$ scans of (0002) peak. The presence of fringes in the (0002) diffraction peak of the ZnO epilayer with a buffer indicates a flat surface and interface. This is also confirmed by AFM measurement. For this sample, the root mean square (rms) value of the surface roughness is less than 8 Å over a $10\ \mu\text{m} \times 10\ \mu\text{m}$ area. The FWHM of the (0002) Ω -rocking-curve (Fig. 5b) of the ZnO layer with an MgO buffer gives an extremely small value of 13 arcsecond when comparing with the 774 arcsecond of the layer without MgO buffer, which indicates finely ordered c -planes as a consequence of a well-controlled layer-by-layer growth, and also implies a very low screw dislocation density. For wurtzite material grown along the c -axis,

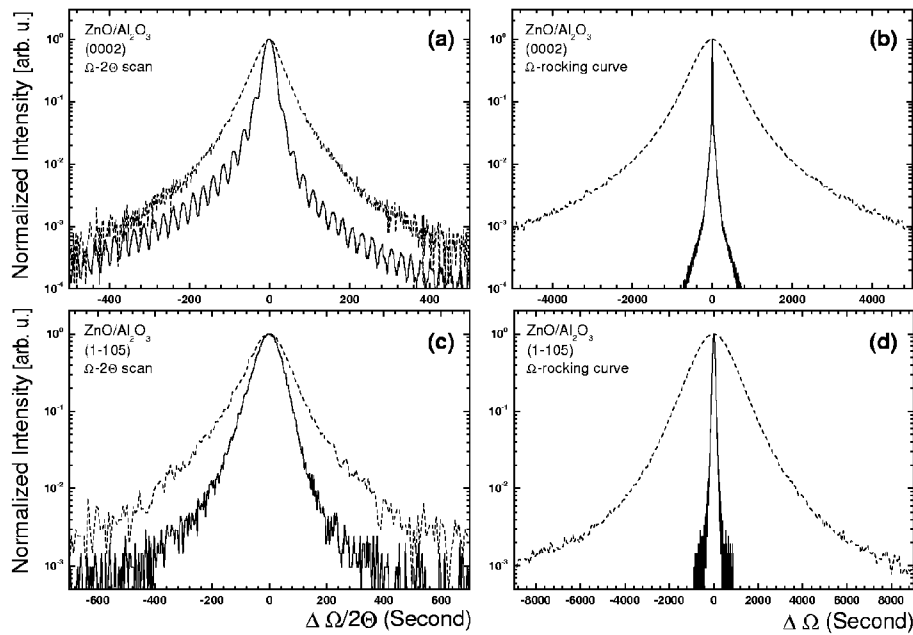


Fig. 5. High-resolution XRD Ω -rocking curves and $\Omega-2\theta$ scans of the ZnO epilayers grown on Al₂O₃ with (solid line) and without (dashed line) an MgO buffer.

the most favorable dislocation is the pure edge dislocation, which causes little crystallographic tilt in the (0001) planes. In order to obtain the information of total dislocation density we examined the (10 $\bar{1}$ 5) asymmetric diffraction peak of ZnO. A Ω -rocking curve is shown in Fig. 5d. The FWHM is 108 arcsecond for the ZnO layer with buffer and 1640 arcsecond for the layer without. In the case of $\Omega-2\theta$, the differences in peak widths are not as large as the rocking-curves. This is because the dislocations have less effect on the inhomogeneous strain than on the mosaicity. All the XRD values shown here are as good as that of GaN grown by MOCVD on Al₂O₃ with a low temperature buffer.

3.2. Polarity controlled ZnO films on Ga-polar GaN templates

Since the polarity of the used GaN templates is Ga-polar (cation-polar), the growth of Zn-polar ZnO films would be possible if we could form “N–Ga–O–Zn” bonding at the interface. However, the formation of such an interface would not be so easy because of reactivity of the GaN surface with oxygen, which leads to the formation of amorphous and/or polycrystalline oxide on GaN [11, 12]. Therefore, in order to form “N–Ga–O–Zn” bonding at the interface and to grow Zn-polar ZnO films on Ga-polar GaN, oxidation problems should be solved. On the other hand, in order to grow O-polar ZnO films on Ga-polar GaN templates, bonding sequences and hence polarity should be inverted.

We have examined two types of pre-growth treatments in order to control the interface bonding between the ZnO epilayer and GaN template: (1) Zn pre-exposure for to achieve Zn-polar growth, (2) O-plasma pre-exposure to form a monoclinic Ga₂O₃ interface layer, which should lead to the O-polar ZnO growth on the Ga-polar GaN template because it has a center of symmetry.

Figure 6 shows RHEED evolutions for the two types of pretreatments. Figures 6a and b show RHEED patterns before and after Zn pre-exposure on the GaN surface. As expected, RHEED did not show any appreciable change in terms of brightness and sharpness of the specular spot and the streaky rods, which indicates small adsorption of Zn as is the case for Zn adsorption onto a GaAs surface [13]. Figures 6c and d show RHEED patterns before and after O-plasma pre-exposure on the GaN surface. On exposing oxygen plasma onto a cleaned GaN surface without Zn pre-exposure, however, the RHEED pattern showed an appreciable change. A decrease in brightness and size of the specular spot, and a change in intensity of streaky rod were observed by O-plasma pre-exposure, which indicate a modification of the GaN surface by O-plasma pre-exposure.

The interface structure of the ZnO/GaN heteroepitaxial layers has been investigated by HRTEM. The interface structure showed a drastic difference between the ZnO films with Zn and O-plasma pre-exposures. No interface layer was formed in between the GaN template and ZnO overlayer in the case of Zn pre-exposure (Fig. 7a), while an interface layer was observed for the O-plasma pre-exposure case (Fig. 7b). As shown in the inset of Fig. 7b, a diffraction pat-

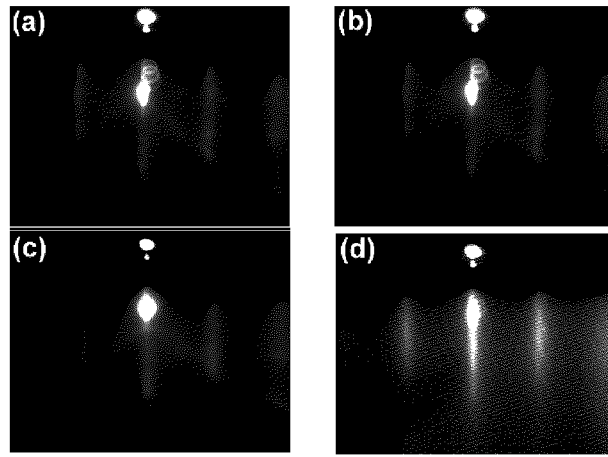


Fig. 6. RHEED patterns in $\langle 11\bar{2}0 \rangle$ azimuth for two types of pretreatments on the GaN surfaces; (a) before and (b) after Zn pre-exposure; (c) before and (d) after O-plasma pre-exposure.

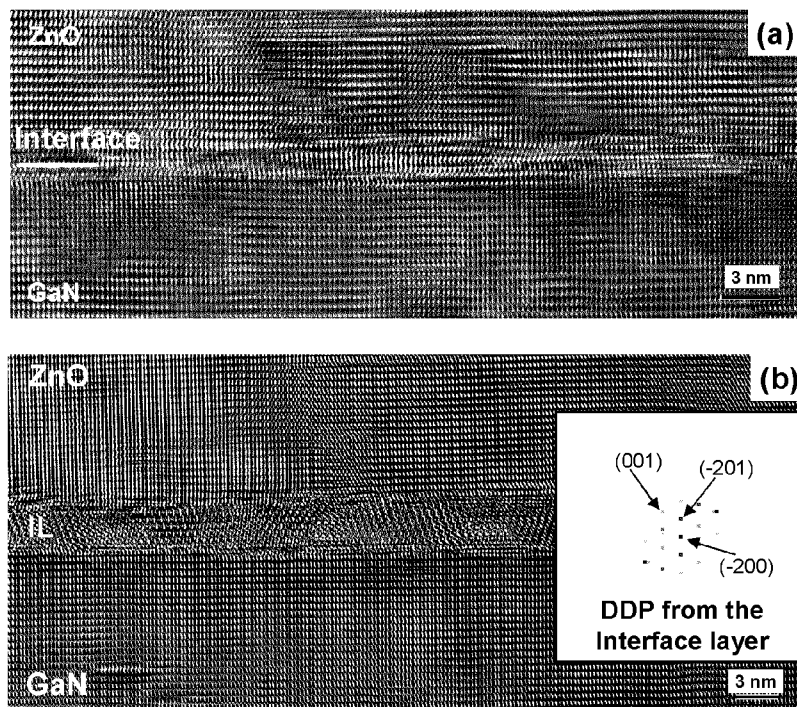


Fig. 7. HRTEM micrographs with the zone axis of $[2\bar{1}1]0$ direction for ZnO films on Ga-polar GaN templates with (a) Zn pre-exposure and (b) O-plasma pre-exposure. The inset in (b) shows a diffraction pattern obtained from the interface layer.

tern obtained by the Fourier transform of the interface layer image showed a single-crystalline pattern. The distances between the diffraction planes marked by the arrows are 0.52 ± 0.01 , 0.53 ± 0.01 and 0.47 ± 0.01 nm. These inter-plane spacings can be assigned to the (001), ($\bar{2}00$), and ($\bar{2}01$) diffraction planes of monoclinic Ga_2O_3 and the zone axis can be assigned to [010]. A detailed analysis of the interface layer suggested that the interface layer was indeed of Ga_2O_3 [14]. The orientation relationship between ZnO, Ga_2O_3 , and GaN would be $\text{ZnO} [2\bar{1}\bar{1}0]/\text{Ga}_2\text{O}_3[010]/\text{GaN}[2\bar{1}\bar{1}0]$ and $\text{ZnO}(0001)/\text{Ga}_2\text{O}_3(001)/\text{GaN}(0001)$. It is noted that both interfaces at $\text{ZnO}/\text{Ga}_2\text{O}_3$ and $\text{Ga}_2\text{O}_3/\text{GaN}$ are sharp with small interface fluctuation.

We have further investigated possible in-plane atomic arrangements at the interface based on the observed orientation relationship using the unit cells of bulk Ga_2O_3 , GaN, and ZnO. Figure 8a shows a Ga_2O_3 unit cell viewed along the [010] direction. A unit cell of Ga_2O_3 contains 8Ga and 12O atoms, and 10 fractional planes along the c -direction. Figure 8b shows a projection view of two Ga_2O_3 unit cells along the direction normal to the (001) plane, in which one hexagonal unit cell of GaN (or ZnO) is overlapped onto a Ga_2O_3 unit cell in accordance with the observed orientation relationship. In this schematic diagram, we have not considered in-plane or out-of-plane rearrangement of atoms at the interface. Although the lattice constant of Ga_2O_3 along the [010] direction (0.304 nm) is

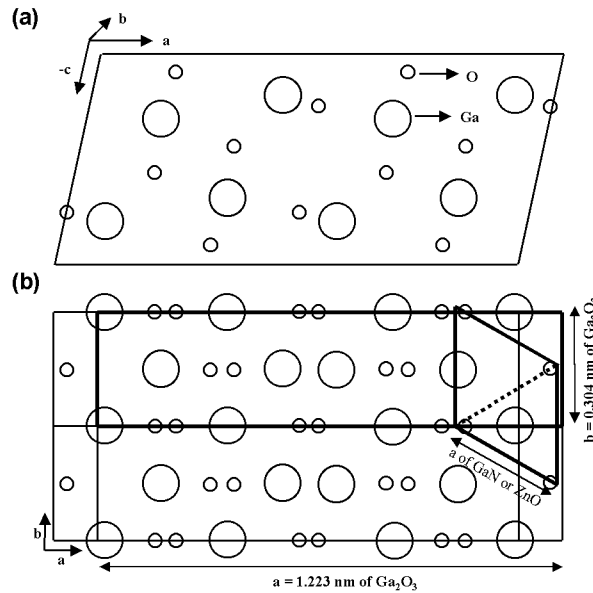


Fig. 8. (a) Ga_2O_3 unit cell viewed along the [010] direction. (b) Schematic diagram showing presumable in-plane lattice matching where Ga_2O_3 unit cell and hexagonal unit of GaN (or ZnO) are overlapped.

slightly smaller than the in-plane lattice constants of GaN (0.319 nm) and ZnO (0.325 nm), the lattice constant of Ga₂O₃ along the [100] direction (1.223 nm) is about four times larger than the corresponding lattice parameters of GaN and ZnO. Because of such large difference in the lattice constant between Ga₂O₃ and ZnO (or GaN), one-to-one direct matching of the three unit cells is impossible. Instead, lattice matching of one unit of Ga₂O₃ along the [100] direction and four unit cells of GaN or ZnO along the [01 $\bar{1}$ 0] direction is possible considering domain matching epitaxy [15]. This situation may facilitate the epitaxial growth of single crystalline ZnO in spite of the large lattice misfit with the Ga₂O₃ interface layer. Thus the lattice misfits along the [010] ($b = 0.304$ nm) and [100] ($a = 1.223$ nm) axes of Ga₂O₃ with the [2 $\bar{1}$ $\bar{1}$ 0] ($a = 0.319$ nm) and [01 $\bar{1}$ 0] ($4\sqrt{3}a/2 = 1.105$ nm) directions of GaN are reduced to -4.7% and 10.7% , respectively. The corresponding lattice misfits between Ga₂O₃ and ZnO are -6.5% and 8.6% , respectively.

In definition, the polarity is caused by the lack of inversion center. If a crystalline layer whose crystal structure has an inversion symmetry is deposited on a surface of a Ga-polar GaN for example, it would be possible to interrupt the propagation of lattice polarity to the overlayer on the interface layer to invert the polarity. Here, it should be strongly noted that the monoclinic Ga₂O₃ interface layer has a center of symmetry, since the space group of Ga₂O₃ is $C2/m$. Therefore, the polarity of the ZnO film without any interface layer grown by Zn pre-exposure shall be Zn-polar. On the other hand, the polarity of the ZnO film with the monoclinic Ga₂O₃ interface layer shall be O-polar, which implies polarity inversion in a wurtzite crystal from cation polar (Ga-polar GaN) to anion polar (O-polar).

The polarities of films and inversion of crystal polarities in the wurtzite structure using an interface layer with a center of symmetry are confirmed by direct determination of the polarities by CBED patterns. Figure 9a shows experimental CBED patterns of an upper ZnO film and a lower GaN one from a Zn pre-exposed sample. The arrow indicates the growth direction. The experimental CBED patterns from the upper ZnO and the lower GaN films are nearly the same. These indicate that the polarity of the upper ZnO film is of Zn-polarity because we have used MOCVD grown Ga-polar GaN templates as substrates and the CBED patterns from GaN and ZnO are most likely very similar considering the structural similarity between ZnO and GaN. Figure 9b shows experimental CBED patterns of an upper ZnO film and a lower GaN one from an O-plasma pre-exposed sample. Note that the experimental CBED patterns from the upper ZnO and the lower GaN films appear opposite. This implies the polarity of the ZnO film is opposite to that of the underlying GaN, and hence the polarity of ZnO film is of O-polar. In order to determine the polarity without ambiguity, comparisons with simulated CBED patterns from ZnO and GaN are performed. Figure 9c shows simulated CBED patterns from wurtzite ZnO and GaN. The simulated patterns correspond to 28 nm and 45 nm thick ZnO and GaN, in which the upward directions are aligned to Zn and Ga-polar, respectively.

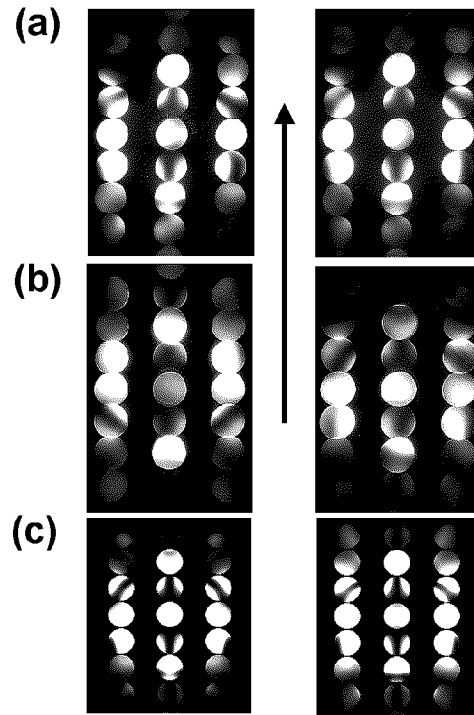


Fig. 9. Experimental CBED patterns of the upper ZnO and lower GaN films from (a) Zn pre-exposed sample and (b) O-plasma pre-exposed sample, and (c) simulated CBED patterns of wurtzite ZnO and GaN with the zone axis of $[2\bar{1}\bar{1}0]$ direction. The arrow indicates the growth direction. The simulated patterns correspond to 28 nm and 45 nm thicknesses of ZnO and GaN, respectively, in which the upward directions are aligned to Zn and Ga polarities.

A comparison of the experimental and simulated CBED patterns directly indicates that the polarity of ZnO film with O-plasma pre-exposure is of O-polar and that of ZnO film with Zn pre-exposure is of Zn-polar, which indicates that we have controlled polarities of wurtzite crystal by engineering the interfaces. We would like to stress again that the present results suggest a generalized method to control the lattice polarity of films by inserting an interface layer with a center of symmetry, thereby the conversion of lattice polarity becomes possible. It should be noted that the proposed method for controlling lattice polarity is more general than any of the previous methods using inverted domains [16, 17].

4. Conclusions

The importance of interface engineering in heteroepitaxy is demonstrated with examples of P-MBE ZnO epitaxy. The heterointerfaces in P-MBE grown

ZnO films on sapphire and Ga-polar GaN template substrates are engineered to improve and to control the properties. The growth of rocksalt structure MgO buffer on Al₂O₃ (0001) is developed for ZnO epitaxy. Lattice misfit for MgO(111)/Al₂O₃(0001) is 8.3%, which implies accommodation of the lattice mismatch of 18.6% for ZnO(0001)/Al₂O₃(0001) by about half and half at ZnO(0001)/MgO(111)/Al₂O₃(0001) interfaces. By using the MgO buffer, the formation of 30° rotated mixed domains is prohibited and two-dimensional layer-by-layer growth of ZnO on sapphire substrate is achieved. High-resolution X-ray diffraction (HRXRD) reveals the superior crystal quality of ZnO films with a MgO buffer.

ZnO/GaN heterointerface without any interface layer is formed by the Zn pre-exposure on the GaN surface, which results in the growth of Zn-polar ZnO films on Ga-polar GaN templates. By the O-plasma pre-exposure on the Ga-polar GaN surface, single crystalline, monoclinic Ga₂O₃ interface layer is formed in between ZnO and GaN. The polarity of ZnO films with the Ga₂O₃ interface layer is O-polar. The CBED result directly shows that the polarity of wurtzite structure is inverted from the cation polar (Ga-polar GaN) to the anion polar (Zn-polar ZnO) by the formation of monoclinic Ga₂O₃, which has a center of symmetry.

References

- [1] D.M. Bagnall, Y.F. Chen, Z. Zhu, T. Yao, S. Koyama, M.Y. Shen, T. Goto, *Appl. Phys. Lett.* **70**, 2230 (1997).
- [2] Z.K. Tang, G.K.L. Wong, P. Yu, M. Kawasaki, A. Ohtomo, H. Koinuma, Y. Segawa, *Appl. Phys. Lett.* **72**, 3270 (1998).
- [3] D.M. Bagnall, Y.F. Chen, Z. Zhu, T. Yao, M.Y. Shen, T. Goto, *Appl. Phys. Lett.* **73**, 1038 (1998).
- [4] H. Wenisch, V. Kirchner, S.K. Hong, Y.F. Chen, H.J. Ko, T. Yao, *J. Crystal Growth* **227-228**, 944 (2001).
- [5] Y. Chen, D.M. Bagnall, H.J. Ko, K.T. Park, K. Hiraga, Z. Zhu, T. Yao, *J. Appl. Phys.* **84**, 3912 (1998).
- [6] S.C. Jain, M. Willander, J. Narayan, R.V. Overstraeten, *J. Appl. Phys.* **87**, 965 (2000).
- [7] Y. Chen, H.J. Ko, S.K. Hong, T. Yao, *Appl. Phys. Lett.* **76**, 559 (2000).
- [8] Y. Chen, S.K. Hong, H.J. Ko, V. Kirshner, H. Wenisch, T. Yao, K. Inaba, Y. Segawa, *Appl. Phys. Lett.* **78**, 3352 (2000).
- [9] S.K. Hong, T. Hanada, H.J. Ko, Y. Chen, T. Yao, D. Imai, K. Araki, M. Shinohara, *Appl. Phys. Lett.* **77**, 3571 (2000).
- [10] S.K. Hong, T. Hanada, H.J. Ko, Y. Chen, T. Yao, D. Imai, K. Araki, M. Shinohara, K. Saitoh, M. Terauchi, *Phys. Rev. B* **65**, 115331 (2002).
- [11] S.D. Wolter, B.P. Luther, D.L. Waltemyer, C. Onneby, S.E. Mohnney, R.J. Molnar, *Appl. Phys. Lett.* **70**, 2156 (1997).
- [12] S.D. Wolter, S.E. Mohnney, H. Venugopalan, A.E. Wickenden, D.D. Koleske, *J. Electrochem. Soc.* **145**, 629 (1998).

- [13] A. Ohtake, S. Miwa, L.H. Kuo, T. Yasuda, K. Kimura, C. Jin, T. Yao, *J. Crystal Growth* **164/185**, 163 (1998).
- [14] S.K. Hong, H.J. Ko, Y. Chen, T. Hanada, T. Yao, *J. Vac. Sci. Technol. B* **18**, 2313 (2000).
- [15] T. Zheleva, K. Jagannadham, J. Narayan, *J. Appl. Phys.* **75**, 860 (1994).
- [16] V. Ramachandran, R.M. Feenstra, W.L. Samey, L. Salamanca-Riba, J.E. Northrup, L.T. Romano, D.W. Greve, *Appl. Phys. Lett.* **75**, 808 (1999).
- [17] L.T. Romano, J.E. Northrup, A.J. Ptak, T.H. Myers, *Appl. Phys. Lett.* **77**, 2479 (2000).